Journal of Alloys and Compounds 656 (2016) 590–597

Contents lists available at ScienceDirect

Journal of Alloys and Compounds

journal homepage: http://www.elsevier.com/locate/jalcom

Studies on the $Zn_xCo_{1-x}S$ thin films: A facile synthesis process and characteristic properties

S.S. Kamble [a, b, *], D.P. Dubal [c], N.L. Tarwal [d, e], A. Sikora [f], J.H. Jang [e], L.P. Deshmukh [a, **]

[a] Thin Film & Solar Studies Research Laboratory, Solapur University, Solapur, 413 255, M.S., India
[b] N.K. Orchid College of Engineering & Technology, Solapur, 413 002, M.S., India
[c] Catalan Institute of Nanoscience and Nanotechnology, CIN2, ICN2 (CSIC-ICN), Campus UAB, E-08193 Bellaterra, Barcelona, Spain
[d] Department of Physics, Lal Bahadur Shastri College, Satara, 415 002, M.S., India
[e] Research Institute for Solar & Sustainable Energies (RISE), Gwangju Institute of Science & Technology (GIST), Gwangju, 500-712, Republic of Korea
[f] Electrotechnical Institute, Division of Electrotechnology & Materials Science, ul. M Skłodowskiej-Curie 55/61, 50-369, Wroclaw, Poland

ARTICLE INFO

Article history:
Received 28 May 2015
Received in revised form
22 September 2015
Accepted 1 October 2015
Available online 9 October 2015

Keywords:
Chemical deposition
$Zn_xCo_{1-x}S$ thin films
XPS
FESEM
AFM
Optical measurements

ABSTRACT

We have synthesized a series of $Zn_xCo_{1-x}S$ ($0 \leq x \leq 0.4$) thin films via the facile and industry preferred chemical deposition. Under the pre-optimized conditions (temperature = 80 ± 0.5 °C, substrate rotation = 65 ± 2 rpm, pH = 9.0 ± 0.1 and duration = 90 min) the deposited films were physically hard, uniform, tightly adherent to the substrate support. As-grown CoS and $Zn_xCo_{1-x}S$ thin films were analyzed for compositional analysis, structural determinations, morphological studies and optical measurements. Elemental analysis determined replacement of Co^{2+} ions from the CoS lattice by Zn^{2+} ions, while a trivial scattering in the virtually constant S-content was observed. Elemental analysis using X-ray photoelectron spectroscopy established chemical states of constituting elements as Co^{2+}, Zn^{2+} and S^{2-}. Hexagonal structure with growth orientation along <101> up to x = 0.25 was observed in the structural studies and above x = 0.25, change in growth orientation along <100> was detected. Enhancement in self-organized growth module ensued the formation of fuzzy microstructure. Improvement in the hillocks with the integration of Zn^{2+} into CoS host was countersigned in the surface topography. The optical transmission spectra of the CoS and $Zn_xCo_{1-x}S$ thin films were analyzed to evaluate the absorption coefficient (α). A systematic increase in α has been found and can be attributed to the creation of more localized states within the band tails due to the existence of defects and disorders.

1. Introduction

The semiconductors and magnetic materials are the key compounds in the high-tech electronic industry. To improve the performance and reduce the size of the devices, enormous work is in progress to combine these two materials. The incorporation of magnetic atoms (transition metal or rare earth atoms) in a host semiconductor lattice is called the dilute magnetic semiconductor (DMS). The use of electron spin with its charge, skills the dilute magnetic semiconductors (DMSs) as an ideal candidates for the spintronic applications.

Zinc sulfide (ZnS) is a II–VI compound semiconductor with a wide bandgap of 3.67 eV (zinc-blende structure) and of 3.90 eV (wurtzite structure) and has an important applications viz. as a phosphor for photoluminescence (PL), electro-luminescence (EL) and cathodoluminescence (CL) devices [1], in light-emitting diodes, electro-optic field detectors, solar cells, lasers and also in spintronic devices [2–5]. Likewise, Cobalt sulfide (CoS) a II–VI group semiconductor also has attracted a considerable attention of the scientific community. It exists in a variety of phases and different stoichiometric compositions, establishing it as one of the trickiest metal chalcogenide to synthesize [6,7]. Its distinctive properties find a lot of places in many applications including solar energy absorbers, magnetic semiconductors, Li-ion batteries and super capacitors [2–10].

Conversely, binary compounds have limited scope in terms of their structural, electronic, optical and magnetic properties. Because of the complex nature of the high-tech photonic, opto-electronic and magneto-electronic devices, it is highly desirable to

* Corresponding author. N.K. Orchid College of Engineering & Technology, Solapur, 413 002, M.S., India.
** Corresponding author. Thin Film & Solar Studies Research Laboratory, Solapur University, Solapur, 413 255, M.S., India.
E-mail addresses: shrishail_kamble@yahoo.co.in (S.S. Kamble), laldeshmukh@gmail.com (L.P. Deshmukh).

http://dx.doi.org/10.1016/j.jallcom.2015.10.011
0925-8388/

search for the substances with tunable variable physical properties. To tune these binary compounds for a specific application, their property engineering can be made feasible by alloying them with an element of known properties.

The Zn–Co–S system thus offers an elucidation to this approach. This half-metallic system can exist in the form of nanoparticles and thin films. However, the studies on thin film form of this material are limited in number. The occasional thin film reports include the synthesis via spray pyrolysis [11], pulsed laser deposition [12] and chemical bath deposition [13,14]. Other methods used for the synthesis of Zn–Co–S films and nanocrystals include: aqueous method [15], refluxing technique [16], precipitation method [17] and hydrothermal approach [18,19]. Recently cobalt has been found to be a prospective doping material in ZnS as Co^{3+} and Co^{2+} doping can result into enhanced photoluminescence [1].

In the pursuit of the magnetic semiconductors, only a handful of work has been carried out on Zn–Co–S system. However, no reports are existing on its chemical growth pertaining to alloyed/mixed systems. Bearing in mind the above particulars, we aimed at the facile synthesis of $Zn_xCo_{1-x}S$ thin films. The strategy of using Zn to substitute Co is from the comparable ionic radii of Co^{2+}(0.72 Å) and Zn^{2+}(0.74 Å) and the same valency state of these two ions [2,3]. With our endless mission of property engineering of the semiconductor thin films using solution growth [8–10,20,21], we hereby, report onto the synthesis of Zn–Co–S thin films and their primitive characteristics.

2. Methods and measurements

2.1. Facile chemical synthesis

Ultrasonically pre-cleaned micro-glass substrates of the dimension 7.2 cm × 0.9 cm × 0.2 cm were utilized for the chemical synthesis of CoS and $Zn_xCo_{1-x}S$ ($0 \le x \le 0.4$) thin films in an alkaline medium. For the synthesis, following procedure was followed: First, 10 ml 1 M $CoSO_4$ solution was taken in a 250 ml beaker. To this, 4 ml TEA was added to form Co(TEA) complex and then 15 ml (25% AR grade) ammonia was added. To this reaction mixture, 10 ml, 1 M thiourea was added and finally total volume of the bath was made 200 ml by adding double distilled water. The resulting pH of the reaction mixture was measured to be 9.0 ± 0.1. A beaker containing reacting solutions was then transferred to the constant temperature oil bath whose temperature was controlled to 80 ± 0.5 °C. The pre-cleaned glass substrates were attached to the substrate holder which was then fixed to a constant speed AC/DC gear motor to set them into rotation (65 ± 2 rpm). For the deposition of $Zn_xCo_{1-x}S$ composites, calculated quantity of 1 M $ZnSO_4$ was added so as to define the value of x between 0.01 and 0.4. After the deposition duration of 90 min, substrates were taken off the beaker, rinsed with double distilled water to remove loosely adhered particles from the surface and then preserved carefully.

2.2. Characterization techniques

The as-grown thin films were then analyzed using different techniques. Terminal layer thicknesses of the films were measured by a Fizeau fringes technique. For the surface wettability test, contact angle measurements based on the sessile-drop method consisting of observation of a water drop through a microscope coupled with goniometer was used. The 2 ml drops were sequentially dropped at different surface positions on the film using a Rame-Hart Inc. model-10 micro-syringe. Contact angles were then determined after 10 s stability period of the droplet. The contents of Co, Zn, and S in the as-grown films were determined by an energy dispersive analysis (EDS) unit attached with FESEM. In the present study, X-ray photoelectron spectroscopy (XPS) was done on a representative sample of composition equal to 0.4. The XPS measurement was performed using a SPECS PHOIBOS 150 hemispherical analyzer (SPECS GmbH, Berlin, Germany) spectrometer with non-monochromatized AlK_α radiation ($h\nu$ = 1486.74 eV) in constant analyzer energy regime (10 eV) with resolution of 1 eV. The crystallographic information on the as-deposited films were obtained using a Bruker X-ray diffractometer (AXS-D8 Advance) in the 2θ range from 10° to 80°. The surface features were observed through a field emission scanning electron microscope (FESEM, Hitachi S-4700, Japan). An atomic force microscope (AFM) Bruker: Innova was used to obtain further morphological insights. Absorption spectra were obtained in the wavelength range from 200 nm to 1600 nm. A BIO-AGE UV–Vis (2800 PC) photo spectrometer was employed for this purpose.

3. Results and discussion

3.1. Reaction kinetics and growth mechanism

CoS thin films deposited optimistically as above were uniform and tightly adherent to the substrate support. The as-grown CoS samples were dark sea-green colored. With the addition of Zn into the CoS film color was found to be changed from dark sea-green to ash-gray as shown in Fig. 1 (Inset). This change in color suggests integration of Zn into the parental CoS structure. Thus, the physical observations coupled with the change in color forms the primal signposts of the formation of the $Zn_xCo_{1-x}S$ thin films. The film thickness measurements showed decrease in the terminal layer thickness, typically from 1354 nm to 691 nm for the composition change from x = 0 to x = 0.4 (Fig. 1). The terminal layer thicknesses are listed in Table 1 for various samples. A growth process for the fabrication of CoS and $Zn_xCo_{1-x}S$ ($0 \le x \le 0.4$) thin films is proposed in-brief as follows:

$$CoSO_4 + n.[\mathrm{TEA}] + \bar{O}H \rightarrow \left[Co(TEA)_n\right]^{2+} + H_2SO_4 + H_2O \quad (1)$$

$$ZnSO_4 + n.[\mathrm{TEA}] + \bar{O}H \rightarrow \left[Zn(TEA)_n\right]^{2+} + H_2SO_4 + H_2O \quad (2)$$

$$(NH_2)_2CS + 2\bar{O}H \leftrightarrow S^{2-} + 2H_2O + CH_2N_2 \quad (3)$$

$$x\left[Zn(TEA)_n\right]^{2+} + (1-x)\left[Co(TEA)_n\right]^{2+} + S^{2-} \rightarrow Zn_xCo_{1-x}S + n(TEA). \quad (4)$$

Initially, TEA forms a complex with Co^{2+}/Zn^{2+}, which decreases the rate of release of free cation concentration in the bath and controls the film growth rate. Simultaneously, S^{2-} anions originates from the hydrolysis of $(NH_2)_2CS$. The reaction between free Co^{2+}/Zn^{2+} cations and S^{2-} anions nucleates and results into a thin $Zn_xCo_{1-x}S$ layer (may be monolayer) on the glass surface. The surface energy of an individual nucleus is high and therefore, they aggregate perpendicularly to the substrate (layer by layer) decreasing their surface energies [22,23]. Thermodynamically, small unstable nuclei grow to large stable seeds through self-arrangement by sharing a common crystallographic alignment and docking of seeds at a planar interface. Eradication of pairs of high surface energies sets up the mainspring for this self-assembled attachment leading to the substantial reduction in the thermodynamic free surface energy. In this spontaneous self-assembly growth, when nuclei/seed approaches close enough to other, it latches mutually by an attractive force. Therefore, as the reaction proceeds, thin strips of Zn–Co–S gets self-aggregated in

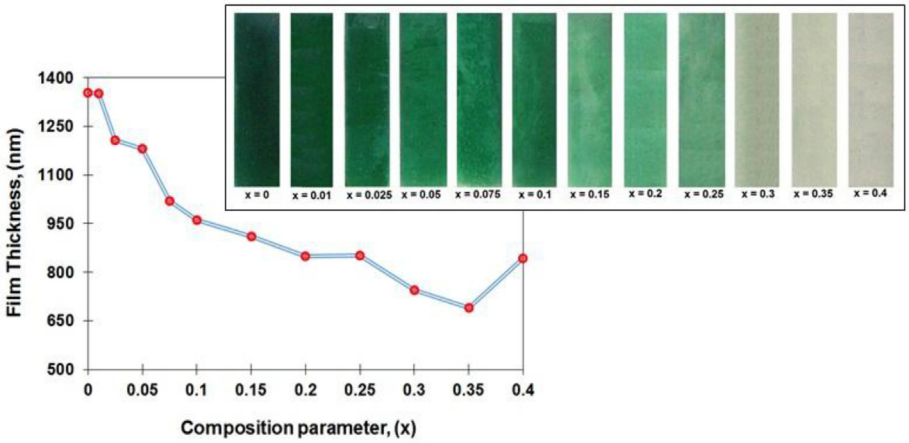

Fig. 1. Variation in terminal layer thickness with Zn concentration in $Zn_xCo_{1-x}S$ thin films (Inset – change in color). (For interpretation of the references to color in this figure legend, the reader is referred to the web version of this article.)

Table 1
Some observations on CoS and $Zn_{1-x}Co_xS$ thin films and EDS analysis of the samples.

Composition (x)	Film thickness (nm)	Angle of contact (θ°)	Atomic%			Zn/Co ratio (film)
			Co	Zn	S	
0	1354	80.0	85.21	–	14.79	–
0.01	1351	60.3	80.68	4.77	14.54	0.06
0.025	1208	58.0	81.46	4.31	14.23	0.05
0.05	1180	56.4	76.52	8.81	14.67	0.12
0.075	1020	59.0	75.41	9.77	14.82	0.13
0.1	960	53.5	71.43	13.51	15.06	0.19
0.15	910	55.0	67.80	16.96	15.24	0.25
0.2	849	55.4	64.31	19.77	15.92	0.31
0.25	851	50.7	61.57	22.24	16.19	0.36
0.3	744	44.3	58.31	25.17	16.52	0.43
0.35	691	48.1	57.12	26.80	16.07	0.47
0.4	843	41.3	55.96	28.11	15.93	0.50

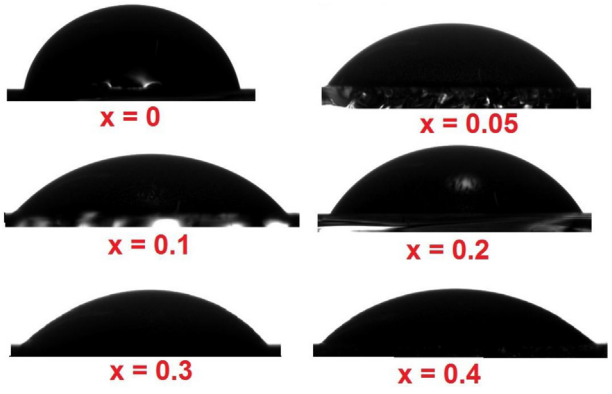

Fig. 2. Representative contact angle measurement results on $Zn_xCo_{1-x}S$ thin films.

the form of fuzzy webbed network perpendicular to the substrate surface minimizing the overall free surface energy.

To understand the growth mechanism further wettability studies were carried out. Wettability of the solid surfaces depends on the surface energy and geometrical features of the solid surface. It is an important measure for thin films since they exhibit a large surface area having large solid–liquid interfacial energies. If the wettability is high, contact angle (θ) will be small and the surface is hydrophilic. On the contrary, if the wettability is low, θ will be large and the surface is hydrophobic. In our case, CoS and $Zn_xCo_{1-x}S$ thin films are of hydrophilic in nature as contact angle (θ) is less than 90°. Typical contact angle measurement results are shown in Fig. 2. With the assimilation of Zn in CoS host lattice, the contact angle decreased and the material tends to be more and more hydrophilic. This specific property is attributed to high surface energy and microstructural amendments of the deposited thin films [24,25] and it is useful for making intimate contact of aqueous electrolyte with the electrode surface in the electrochemical PV-cells. The contact angles of the as-deposited CoS and $Zn_xCo_{1-x}S$ thin films are cited in Table 1.

3.2. Composition determination

3.2.1. Energy dispersive X-ray spectroscopy (EDS)

An energy dispersive X-ray analysis was conducted on these samples to determine the qualitative measure of Co^{2+} substitution by Zn^{2+} assimilation. The deposits at our experimental conditions were S-deficient and for x = 0, deposited CoS thin film is ≈ 85% Co-rich as observed in earlier reports also [20]. The analysis further showed that Co^{2+} from the CoS lattice has been replaced by Zn^{2+} ions and with the increasing Zn-content in the chemical bath, content of Zn in the film increased. Correspondingly, Co-content in the film decreased, whereas S-content remained almost constant throughout the composition range. Table 1 shows the contents of Co, Zn and S in the different samples. Fig. 3A shows the EDS diffractograms for the two typical samples whereas Fig. 3B represents their 3D representation. In the near vicinity of x = 0.1–0.15, the

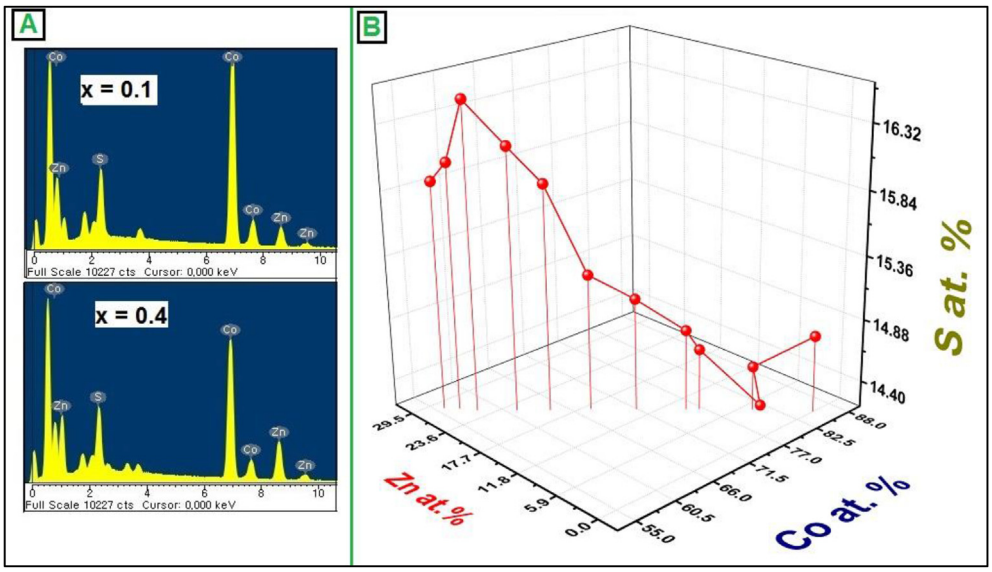

Fig. 3. **(A)** Typical EDAX pattern for x = 0.1 and 0.4, **(B)** 3D plot of atomic% of Co, Zn and S as revealed from EDS studies.

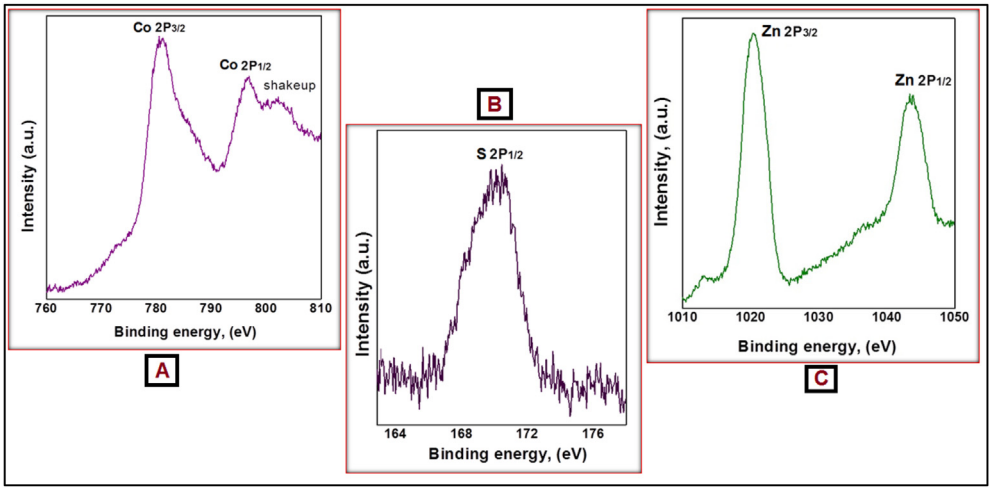

Fig. 4. Core level spectra for **(A)** Co 2p **(B)** S 2p and **(C)** Zn 2p.

samples are near stoichiometric. Whereas, stoichiometry deviates for higher values of Zn in CoS.

3.2.2. *X-ray photoelectron spectroscopy (XPS)*

The XPS survey spectrum of one of the representative Zn(CoS) samples (x = 0.4) was recorded in the BE range from 0 to 1400 eV. In the obtained overview spectra, apart from for the lines of the main elements; carbon and oxygen were also detected. To extract the information about chemical states of the elements of interest, narrow regions of their core level spectra were analyzed, original XPS spectra being de-convoluted on separate components. Fig. 4A highlights the narrow scan of Co 2p core-level photoemission spectrum. The Co 2p core level spectrum is characterized by two components appearing due to spin-orbital splitting (Co $2p_{3/2}$ and Co $2p_{1/2}$) and shake-up satellites. The binding energy of Co $2p_{3/2}$ and Co $2p_{1/2}$ is located at 781.33 eV and 796.83 eV, respectively. The large spin orbital splitting of 15.53 eV between Co $2p_{3/2}$ and Co $2p_{1/2}$ with that of pure Co metal (15.05 eV) indicates +2 oxidation state of Co ions. The observation of two shake-up satellites on the higher binding energy is a typical characteristic of high spin Co^{2+} [26] originating from the charge-transfer band structure characteristic of the 3d transition metal monoxides [27]. The binding energy of Co 2p along with the shake-up peaks could be well fitted to the standard spectrum for CoO film (Co^{2+}) [28]. Hence, it is concluded that the cobalt is in the +2 oxidation state.

Whereas, narrow scan of S 2p core level (Fig. 4B) indicated the presence of S^{2-} chemical state with binding energy of 169.86 eV which is in consonance with the standard value of S^{2-} chemical state. In as-grown Zn(CoS) thin films, because of the strong spin–orbit coupling, the Zn 2p peak (Fig. 4C) also splits into two (Zn $2p_{3/2}$ and Zn $2p_{1/2}$) at 1020.51 eV and 1043.62 eV respectively with a doublet separation of 23.11 eV, which is consistent with the standard separation of 23.1 eV corresponding to Zn^{2+} [26]. Thus, the XPS studies established chemical states of Co, Zn and S as Co^{2+}, Zn^{2+} and S^{2-}.

3.3. *Structural analysis*

The X-ray diffractograms were obtained for these composite films in the 10°–80° 2θ range with Cu Kα radiation (1.5406 Å). The

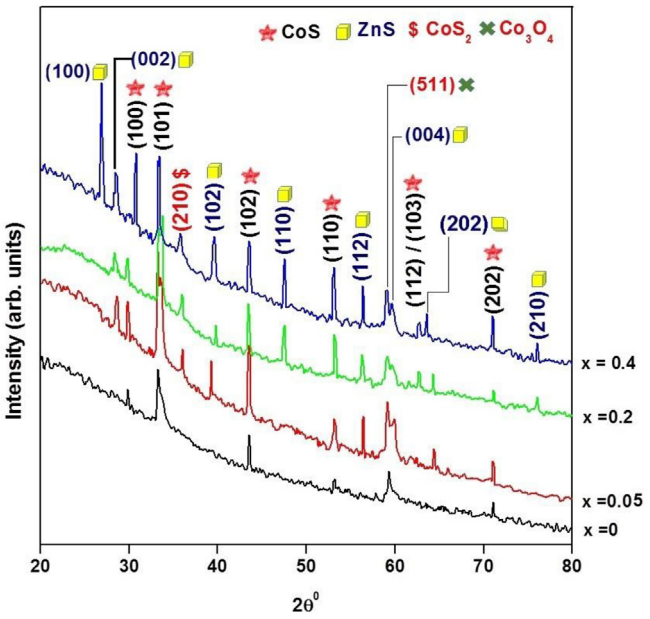

Fig. 5. Typical X-ray diffractograms of $Zn_xCo_{1-x}S$ thin films.

diffractograms (Fig. 5) were further analyzed to compute the interplanar distances (d), intensities of reflections (I/I_{max}), lattice parameters (a and c), and average crystallite size. Strong and sharp signals indicated well-crystallized hexagonal structure with dominant growth orientation along (101) direction. For this reflection, d is found to be continuously decreased from 2.691 Å to 2.663 Å for the change of x from 0 to 0.15, whereas I/I_{max} is 100% up to $x = 0.25$ and thereafter decreased to around 60% for higher x values. The observed intensities of reflections, d-values and lattice parameters have good consonance with the JCPD values [29]. The existence of two minor reflections, (210) and (511) corresponding to formation of CoS_2 and Co_3O_4 phases, have also been detected. Owing to the strong oxygen affinity of CoS material it is practically difficult to avoid oxygen related phases in thin films [21]. The analysis further showed noticeable shift in the position of (101) peak; for the $0 \leq x \leq 0.15$ range, it is right shifted, whereas left shifted for $0.2 \leq x \leq 0.4$. It is therefore expected that a significant change in the lattice parameters could be induced by the introduction of Zn into CoS. The above results can be understood as the zinc integrates considerably into CoS host lattice (EDS studies). The lattice parameters a and c were therefore calculated for the film structures and are documented in Table 2. Both a and c are found to be increased continuously with the integration of Zn into the host CoS. The ratio c/a is almost constant. Thus continuous changes in d, lattice parameters 'a' and 'c' and structural similarity suggest that there is a formation of ternary alloy of the type Zn–Co–S over a $0 \leq x \leq 0.15$ composition range [30,31]. Beyond this composition range, separate phase formation has been detected.

Owing to the above facts, we have synthesized the variable composition films and it is seen that the lattice parameters a and c were found to be increased with increase in the film composition x, whereas d decreased with increase in x up to $x = 0.15$ and then remained more or less constant. At higher impurity levels, the above parameters tend to saturate around their standard values. The crystallite sizes were then determined for all the film structures using the Scherrer's relation. The size of the crystallite is in the nano range and found to be enhanced with Zn-content up to $x = 0.4$. Integration of Zn into the parent CoS increases the lattice distortion which further increases the crystallite size and perchance amend the morphological details.

3.4. Morphological analysis

Surface morphology of a thin film is dependent on various growth parameters [21]. In our case mechanical agitation and thermal assistance catalyzed into the primary growth of the thin films onto the substrate surface and provides nucleation centers for secondary growth [21]. The surface morphologies of the different films were therefore viewed through the scanning electron and atomic force microscopes. FESEM micrographs of Fig. 6 (as-deposited) shows the surface morphologies of the CoS and $Zn_xCo_{1-x}S$ samples. The micrographs revealed complex multifaceted webbed network of elongated crystallites resembling like the flakes with uniform substrate surface coverage. In general, film microstructures consist of a fuzzy network of elongated crystallites reminiscent of flakes with polygon shaped vacant spaces between them. Such porous thin films are of prime importance as electrode material in super capacitive applications [8,9]. Inconsequence overgrowth with the formation of a sluggish layer over the entire microstructure and a sort of recrystallization has also been evidenced for lower concentration of Zn in CoS ($x = 0–0.075$). For succeeding compositions ($x = 0.1–0.4$) micrographs showed clear multifaceted complex network. Further, it is also to be noted that, with the increase in Zn into CoS framework, an individual

Table 2
Some observations on XRD, AFM and optical studies of CoS and $Zn_{1-x}Co_xS$ thin films.

Composition, (x)	Lattice parameters			(101) CoS plane		Avg. crystallite size ($\overline{D}$), (nm)	Avg. roughness R_a, (nm)	RMS roughness Rq, (nm)	$\alpha \times 10^4$, (cm^{-1})	Band gap, (eV)
	a (Å)	c (Å)	c/a	d_{101}, (Å)	Intensity (%)					
0	3.432	5.784	1.685	2.691	100	13	38.67	54.81	2.955	1.59
0.01	3.439	5.788	1.683	2.677	100	16	51.80	67.60	2.962	1.76
0.025	3.442	5.810	1.688	2.676	100	23	99.62	136.29	3.312	1.98
0.05	3.445	5.868	1.703	2.674	100	27	138.86	171.37	3.134	2.20
0.075	3.446	5.868	1.703	2.669	100	27	144.55	179.49	3.920	2.21
0.1	3.449	5.871	1.702	2.668	100	34	183.28	222.27	4.166	2.23
0.15	3.451	5.891	1.707	2.667	100	36	185.50	247.29	4.739	2.44
0.2	3.457	5.903	1.707	2.673	100	38	216.10	258.24	4.987	2.29
0.25	3.460	5.911	1.708	2.674	100	38	242.46	303.54	4.619	2.36
0.3	3.462	5.907	1.706	2.675	63	39	256.80	324.79	4.833	2.44
0.35	3.463	5.911	1.707	2.676	61	41	294.71	366.71	4.410	2.44
0.4	3.465	5.925	1.710	2.676	66	42	424.02	525.41	3.742	2.50
	CoS	$a_{standard} = 3.440$ Å $c_{standard} = 5.790$ Å								

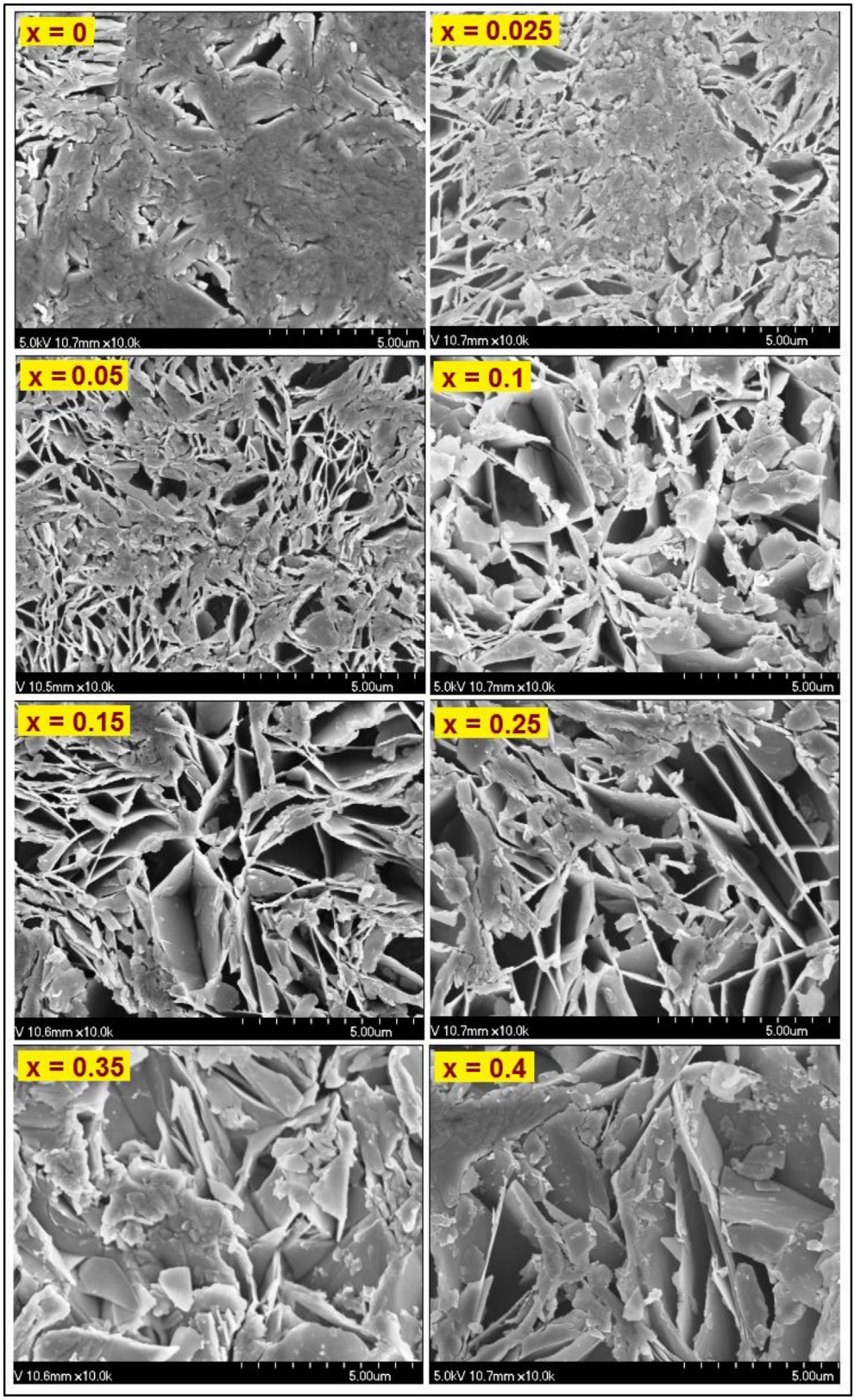

Fig. 6. FESEM micrographs of the as-grown CoS and few of the typical $Zn_xCo_{1-x}S$ samples.

crystallite grows further along with the polygon shaped voids in between them and a considerable improvement in microstructure has been observed.

The samples were also viewed through an atomic force microscope. Fig. 7 shows different three dimensional surface topographies (10 μm × 10 μm) of the as-obtained thin films. The

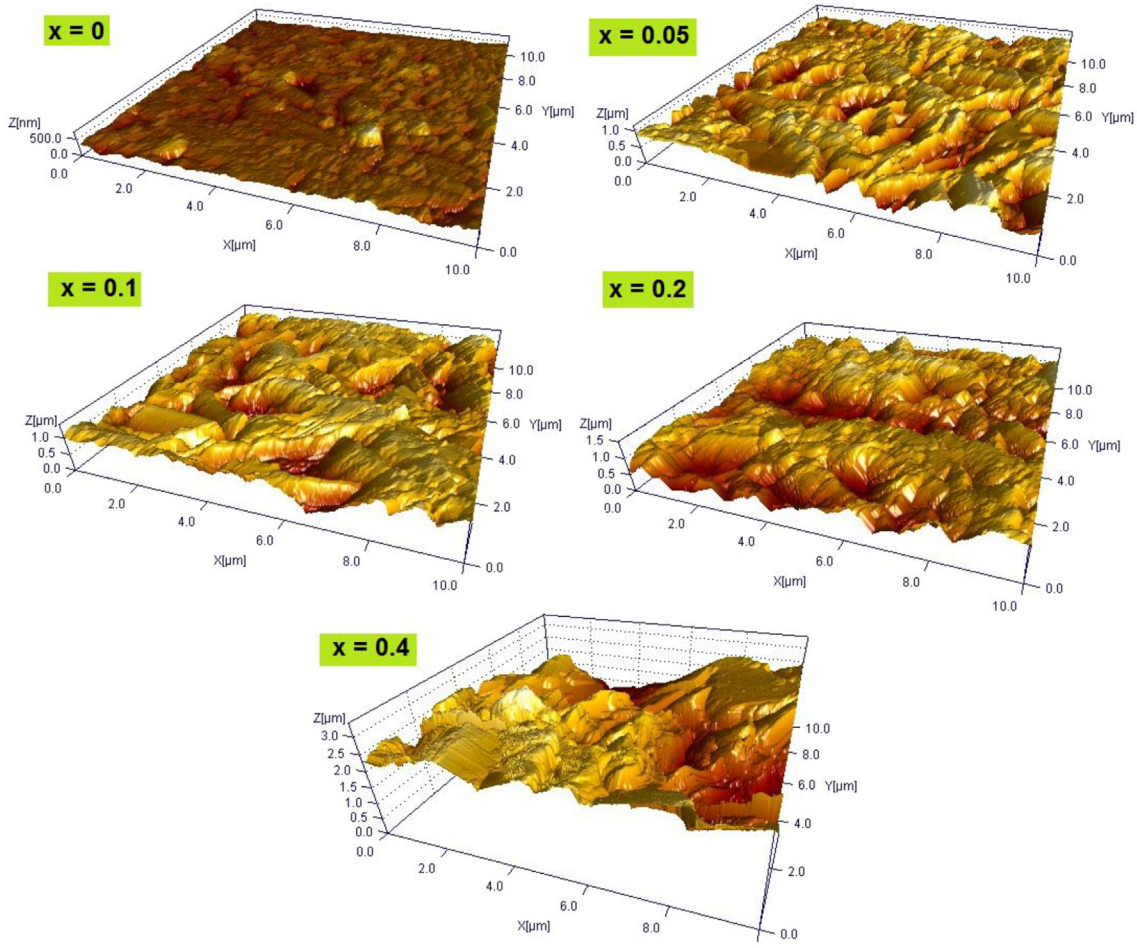

Fig. 7. Representative 3D AFM topographs of the as-deposited CoS and $Zn_xCo_{1-x}S$ thin films.

topographs showed that, as-grown thin films have covered entire substrate surface with good adherence to the substrate support. Surface topographies of Zn(CoS) thin films consist of the hillocks and valleys suggesting its crystalline nature. Height of the hillocks specifies the crystalline nature whereas, the valleys identify the inter-granular spacing. As an inclusive study, few of the AFM parameters were determined and listed in Table 2. From the AFM images shown in Fig. 7, it is seen that the growth is influenced by the extent of Zn in the reaction bath. The surface topographs further revealed improvement in hillocks with the accumulation of Zn into the CoS matrix, crafting valleys and hence surface tends to be rough. The topographs further showed enhanced crystalline nature with Zn integration and as a result one could see increase in average and RMS roughnesses. The increase in RMS roughness can be attributed to the enhanced grain growth as evidenced from the SEM micrographs. For small values of x, film roughness is fairly low with shallow valleys. At moderate levels of Zn addition into CoS structure, roughness also goes on increasing with superficial valleys. As the Zn content in the bath is increased further (x = 0.3–0.4), surface becomes rougher and eventually has a cavernous appearance. Variation in the RMS roughness is found to be interconnected with the angle of contact and wettability of the thin films [24,25]. More is the RMS roughness, smaller is the angle of contact and consequently more is the hydrophilicity of the as-deposited thin films.

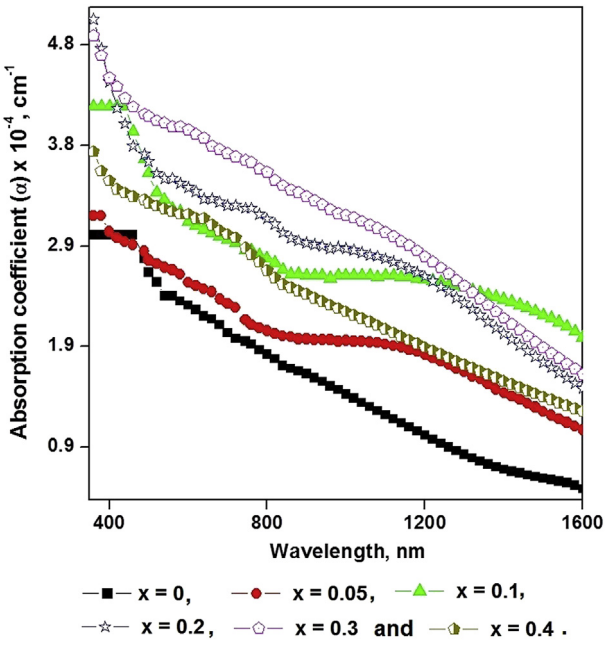

Fig. 8. Variation of absorption coefficient (α) vs wavelength (λ) for six representative Co–Zn–S thin film structures.

3.5. Optical studies

An ideal semiconductor with no defects and impurities has an intrinsic absorptivity in the 10^2–10^4 cm^{-1} range at wavelengths between Urbach tail of electronic edge at the short wavelength limit and the phonon edge at the long wavelength limit [20,31]. Introduction of transition metals into semiconductors arises not only magnetism related phenomenon but other changes as well. Specifically, addition of transition metal impurities can alter the electronic band structure [9,10,31–33]. The optical absorption spectra of the CoS and $Zn_xCo_{1-x}S$ thin films were therefore obtained in the range of wavelengths from 200 nm to 1600 nm. The spectra were analyzed to evaluate the absorption coefficient which is plotted against wavelength (λ) for six representative samples and are shown in Fig. 8. It is found that absorption coefficients (α) of both pure CoS and $Zn_xCo_{1-x}S$ samples are of the order of 10^4 cm^{-1}. A systematic increase in α may be attributed to the creation of more localized states within the band tails of valence and conduction bands due to the existence of defects and disorders [31–33]. The lower wavelength range shift in the absorption coefficient with increase in Zn content can be explained with sp-d exchange interaction between the band electrons in CoS and localized d electrons in Zn^{2+} [8,9,32,34,35]. In the present system, zinc plays a two-fold role [34,35]: first, it occupies partially vacant Co sites and manipulates the defect states and secondly, it forms a semiconducting alloy whose composition controls the band structure and lattice spacing. The values of the optical band gaps were then calculated from the best straight line fits in the $(\alpha h\nu)^2$ versus hν plots (figure not shown) and corresponding band gaps were obtained from the extrapolation of the straight portion of the graph at $(\alpha h\nu)^2 = 0$ and cited in Table 2. From the measured values, it is observed that the band gap energy increased with the added Zn-concentration.

4. Conclusions

Growth of CoS and $Zn_xCo_{1-x}S$ thin films from precursors containing Co^{2+}, Zn^{2+} and S^{2-} ions in an aqueous alkaline (pH = 9.0 ± 0.1) medium is made feasible. Change in color with increase in hydrophilicity support assimilation of Zn into CoS. EDS analysis revealed S^{2-} deficient nature of the as-grown CoS and Zn–Co–S thin films. Replacement of Co^{2+} to accommodate Zn^{2+} into CoS host lattice is observed. Co^{2+}, Zn^{2+} and S^{2-} oxidation states were established by an elemental XPS analysis. Structural studies revealed polycrystalline nature of the thin films with hexagonal structure. Growth orientation is along <101>. The shift in 2θ values, continuous change in lattice parameters and optical band gap point out the solubility of Zn^{2+} into CoS up to x = 0.15. Morphological progression from fuzzy network to firm structure with the incorporation of Zn in CoS is observed through the FESEM. AFM topographs revealed improvement of the hillocks with the accumulation of Zn into the CoS matrix, crafting cavernous valleys and increasing RMS roughness. AFM topographs support the conclusions drawn from the FESEM and a diligent relationship is found between contact angle and RMS roughness. Variation in the absorption coefficient is attributed to the systematic increase in the localized states due to the existence of defects and disorders. The optical band gap is found to be increased with the addition of Zn^{2+} in CoS host and transitions are of the direct type.

References

[1] R. Sarkar, C.S. Tiwary, P. Kumbhakar, A.K. Mitra, Phys. B 404 (2009) 3855–3858.
[2] A.D. Mani, M. Deepa, P. Ghosal, C. Subrahmanyama, Electrochim. Acta 139 (2014) 365–373.
[3] S. Sambasivam, D.P. Joseph, J.G. Lin, C. Venkateswaran, J. Solid State Chem. 182 (2009) 2598–2601.
[4] T. Liu, H. Ke, H. Zhang, S. Duo, Q. Sun, X. Fei, G. Zhou, H. Liu, L. Fan, Mater. Sci. Semicond. Process. 26 (2014) 301–311.
[5] C. Song, B. Chen, Y. Chen, Y. Wu, Z. Zhuang, X. Lu, X. Qiao, X. Fan, J. Alloy. Compd. 590 (2014) 546–552.
[6] R.L. Gunshor, L.A. Kolodziejski, A.V. Nurmikko, N. Otsuka (Eds.), Semiconductors and Semimetals, vol. 33. Chapter 6. Molecular-Beam Epitaxy of II-VI Semiconductor Microstructures, 338–403.
[7] K. Qi, J. Yu, K. Chen, Cryst. Res. Technol. 48 (2013) 1083–1086.
[8] S.T. Mane, P.C. Pingale, S.A. Lendave, V.S. Karande, L.P. Deshmukh, M. Sharon, Electrochim. Acta 102 (2013) 113–119.
[9] S.T. Mane, P.C. Pingale, R.V. Suryawanshi, V.S. Karande, L.P. Deshmukh, M. Sharon, Electrochim. Acta 114 (2013) 494–499.
[10] S.S. Kamble, A. Sikora, S.T. Pawar, R.C. Kambale, N.N. Maldar, L.P. Deshmukh, J. Alloy. Compd. 631 (2015) 303–314.
[11] I. Polat, S. Aksu, M. Altunbas, E. Bacaksiz, Mater. Chem. Phys. 130 (2011) 800–805.
[12] S.P. Patel, J.C. Pivin, A.K. Chawla, R. Chandra, D. Kanjilal, L. Kumar, J. Magn. Magn. Mater. 323 (2011) 2734–2740.
[13] W.J. Fang, Y.S. Liu, B.Z. Guo, L. Peng, Y.B. Zhong, J.C. Zhang, Z.J. Zhao, J. Alloy. Compd. 584 (2014) 240–243.
[14] L.J. Tang, G.F. Huang, Y. Tian, W.Q. Huang, M.G. Xia, C. Jiao, J.P. Long, S.Q. Zhan, Mater. Lett. 100 (2013) 237–240.
[15] M.S. Akhtar, M.A. Malik, S. Riaz, S. Naseem, P. O'Brien, Mater. Sci. Semicond. Process. 30 (2015) 292–297.
[16] B. Poornaprakash, D.A. Reddy, G. Murali, N.M. Rao, R.P. Vijayalakshmi, B.K. Reddy, J. Alloy. Compd. 577 (2013) 79–85.
[17] P. Yang, M. Lu, D. Xu, D. Yuan, C. Song, G. Zhou, J. Phys. Chem. Solids 62 (2001) 1181–1184.
[18] L. Liu, L. Yang, Y. Pu, D. Xiao, J. Zhu, Mater. Lett. 66 (2012) 121–124.
[19] J.S. Jang, E.S. Kim, S.H. Choi, D.H. Kim, H.G. Kim, J.S. Lee, Appl. Catal. A Gen. 427– 428 (2012) 106–113.
[20] S.T. Mane, S.S. Kamble, L.P. Deshmukh, Mater. Lett. 65 (2011) 2639–2641.
[21] S.S. Kamble, A. Sikora, S.T. Pawar, N.N. Maldar, L.P. Deshmukh, J. Alloy. Compd. 623 (2015) 466–472.
[22] F.C. Eze, C.E. Okeke, Mater. Chem. Phys. 47 (1997) 31–36.
[23] A.A. Carbajal Readigos, V.M. Garcia, O. Gomezdaza, J. Campos, M.T.S. Nair, P.K. Nair, Semicond. Sci. Technol. 15 (2000) 1022–1029.
[24] C. Carraro, O.W. Yauw, M.M. Sung, R. Maboudian, J. Phys. Chem. B 102 (1998) 4441–4445.
[25] J.D. Miller, S. Veeramasuneni, J. Drelich, M.R. Yalamanchili, G. Yamauchi, Polym. Eng. Sci. 36 (1996) 1849.
[26] J.F. Moulder, W.F. Stickle, P.E. Sobol, K.D. Bomden, J. Chastain (Eds.), Handbook of X-ray Photoelectron Spectroscopy, Perkin-Elmer, Eden Prairie, Minnesota, 1992.
[27] G.A. Garson, M.H. Nassir, M.A. Langell, J. Vac. Sci. Technol. A 14 (1996) 1637.
[28] M.C. Biesinger, B.P. Payne, A.P. Grosvenor, L.W.M. Lau, A.R. Gerson, R.St.C. Smart, Appl. Surf. Sci. 257 (2011) 2717–2730.
[29] JCPDS Cards: CoS-03-065-0407, CoS-03-065-3418, CoS-01-075-0605, CoS2-00-041-1471, ZnS-01-079-2204, ZnS-01-080-0007.
[30] G.B. Sakr, I.S. Yahia, G.M. El-Komy, A.M. Salem, Surf. Coat. Technol. 205 (2011) 3553–3558.
[31] A.N. Chattarki, L.P. Deshmukh, J. Alloy. Compd. 597 (2014) 223–229.
[32] V.S. Karande, S.H. Mane, V.B. Pujari, L.P. Deshmukh, Mater. Lett. 59 (2005) 148–152.
[33] S.A. Lendave, P.C. Pingale, L.P. Deshmukh, Rare Metal Mater. Eng. 41 (2012) 43–46.
[34] S. Kumar, P. Sharma, V. Sharma, J. Nanopart. Res. 15 (2013) 1662.
[35] J. Luengo, N.V. Joshi, Mater. Lett. 26 (1996) 47–50.